Reinforcement layout design for concrete structures based on continuum damage and truss topology optimization

Oded Amir and Ole Sigmund
Department of Mechanical Engineering, Technical University of Denmark

Abstract

This article presents a new procedure for the layout design of reinforcement in concrete structures. Concrete is represented by a gradient-enhanced continuum damage model with strain-softening and reinforcement is modeled as elastic bars that are embedded into the concrete domain. Adjoint sensitivity analysis is derived in complete consistency with respect to path-dependency and the nonlocal model. Classical truss topology optimization based on the ground structure approach is applied to determine the optimal topology and cross-sections of the reinforcement bars. This approach facilitates a fully digital work flow that can be highly effective, especially for the design of complex structures. Several test cases involving two- and three-dimensional concrete structures illustrate the capabilities of the proposed procedure.

Keywords: Reinforced concrete; Topology optimization; Continuum damage; Truss optimization

1 Introduction

Structural optimization techniques are now considered an integral part of the design process in various industries, e.g. the automotive and aerospace industries. In particular, topology optimization is emerging as a generic digital design tool that can be utilized in a wide range of engineering fields, spanning from nano-scale photonics up to furniture and buildings [Sigmund and Bendsøe, 2004, Dombernowsky and Søndergaard, 2009, Stromberg et al., 2011]. Up to date, optimal design had little impact on traditional structural engineering as practiced in the construction industry. Considering structural design with reinforced concrete, optimal design is exceptionally challenging due to the difficulty in combining numerical optimization tools with accurate constitutive models. Furthermore, applying continuum topology optimization procedures is difficult because of the two distinct physical scales involved: reinforcement is achieved by inserting a very small volumetric ratio of discrete steel bars into the continuum concrete.

The focus of the current study is on the design of the so-called 'D-regions' in structural concrete where the strain distribution is nonlinear. In practice, strut-and-tie models are widely applied for positioning and quantifying the reinforcement in such regions of the structure [Marti, 1985, Schlaich et al., 1987]. This is opposed to 'B-regions' where beam theory and cross-sectional analysis are sufficient for determining the necessary reinforcement. The strut-and-tie approach offers a simple model for identifying the flow of forces in a cracked concrete continuum and is incorporated into major international building codes. The method's main drawbacks are time-consuming implementation; lack of specialized computer software for practical design; as well as the difficulty in considering serviceability requirements such as deflections and crack widths [*fib* Task Group 4.4, 2008]. In the context of utilizing optimization in reinforced concrete design, linear-elastic continuum topology optimization was proposed as a means of automatically generating strut-and-tie models [Liang et al., 2000]. More recently, Victoria et al. [2011] extended this idea by considering different material properties in tension and compression; and Moen and Guest [2010] suggested truss topology optimization as a basis for generating the strut-and-tie model. However, these contributions do not address the complete design problem: further interpretation is required in order to proceed with solving the model and computing the amount of reinforcement. With respect to B-regions in reinforced concrete such as beams, columns and

frames, structural optimization based on cross-sectional forces resulting from frame analysis was addressed by numerous investigators since the 1970's but is beyond the scope of this article.

Significant advancements in nonlinear finite element analysis of reinforced concrete structures facilitate the future development of computer-based automated design tools [*fib* Task Group 4.4, 2008]. It is the purpose of this article to discuss a methodology that suggests a step forward towards digital design of reinforced concrete. The procedure utilizes truss topology optimization for determining the layout of reinforcement in D-regions of concrete structures. The key point is the combination of a continuum damage model for concrete together with the embedded reinforcement formulation that enables the representation of discrete reinforcement bars (rebars). As will be clarified throughout the article, a fully digital work flow can be established, relying only on a finite element package capable of: nonlinear analysis; topology optimization; and basic drawing. Such a procedure is especially attractive in the design of complex 2-D and 3-D structures where strut-and-tie models are not easily realized.

In various aspects, the present study is inspired by and related to recent developments by Kato et al. [2009] and Kato and Ramm [2010] regarding optimization of fiber reinforced concrete. It differs mainly in the aim to generate general optimized layouts as opposed to sizing and shape optimization of predefined reinforcement layers. We use the same continuum damage model for concrete [Peerlings et al., 1996] and the same approach to embedded reinforcement modeling, proposed initially by Phillips and Zienkiewicz [1976]. Kato et al. [2009] considered also a bond-slip interface model which is not included in the present approach. On the other hand, the sensitivity analysis procedure is completely consistent and accounts also for the influence of the non-local strains in the damage model, which were previously neglected for simplicity.

The article is organized as follows: first the finite element analysis is described in Section 2, with emphasis on the continuum damage model and on the embedded formulation in the context of truss topology optimization. Adjoint sensitivity analysis is discussed in detail in Section 3. In Section 4 we present the optimization problem formulation followed by a detailed case study of a simple 2-D deep beam. Several demonstrative examples of optimized rebar layouts in two and three dimensions are presented in Section 5. Finally, current results and future work are discussed in Section 6

2 Finite element modeling

2.1 Continuum damage model for concrete

In the current study, plain concrete is modeled as a strain-softening damaged continuum following Peerlings et al. [1996]. In the context of concrete modeling for structural optimization, this model was recently utilized successfully in several studies [Kato et al., 2009, Kato and Ramm, 2010]. The principal ingredients and assumptions of the constitutive model are outlined in this section for the purpose of completeness. Large deformations are not considered in the current study, meaning we assume small displacements and small strains.

Damage is assumed to be isotropic and therefore the process is defined by a single scalar variable D, where $0 \leq D \leq 1$. The stress-strain relation is given by

$$\sigma = (1-D)\mathbf{C} : \varepsilon$$

where σ is the stress tensor, $\mathbf{C}$ is the elastic constitutive tensor and ε is the strain tensor. The product $\mathbf{C} : \varepsilon$ is usually named the *effective stress* which acts on the actual resisting undamaged area (see for example [Lemaître and Desmorat, 2005] for an introduction to damage mechanics). The evolution of damage is governed by the history parameter κ. In the current study we utilize an exponential damage law [Mazars and Pijaudier-Cabot, 1989]

$$D = 1 - \frac{\kappa_0}{\kappa}\left(1 - \alpha + \alpha \exp^{-\beta(\kappa-\kappa_0)}\right)$$

where κ_0 is a threshold value corresponding to the initiation of damage and α and β are material constants. The damage law and the resulting uniaxial stress-strain curve are plotted in Fig. 1 for the parameter values

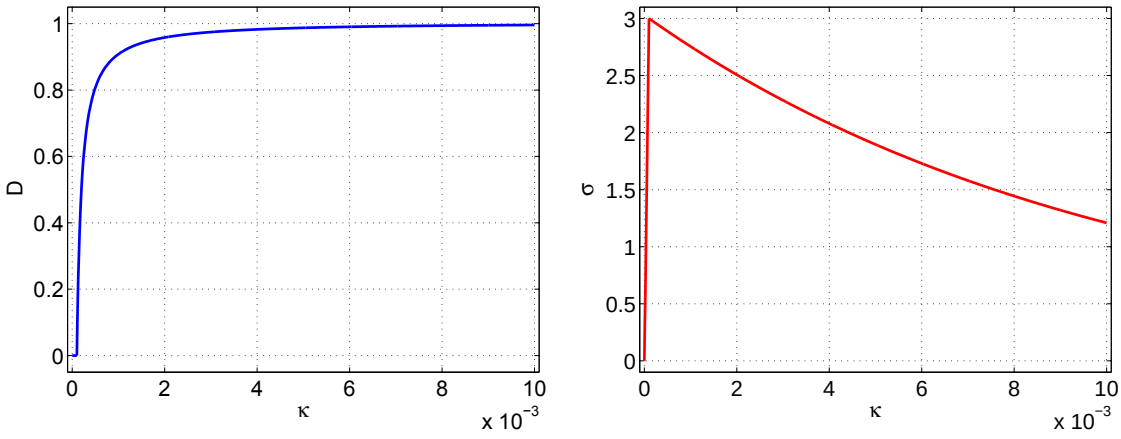

Figure 1: Exponential damage law and resulting strain-softening curve

$\kappa_0 = 1 \times 10^{-4}$, $\alpha = 0.95$, $\beta = 100$ and Young's modulus of 3×10^4. The history parameter corresponds to the extremal deformation of the material, measured in the multiaxial case by an equivalent strain. In the current study the equivalent strain measure resembles the Drucker-Prager yield function [Drucker and Prager, 1952]

$$\varepsilon_{eq} = \sqrt{3J_2} + mI_1$$

where J_2 is the second invariant of the deviatoric strain; I_1 is the trace of the strain tensor; and m is a material property that can be related to the ratio of strengths in uniaxial tension and compression. This equivalent strain measure is essentially used in order to detect the initiation of damage: once the equivalent strain at a certain material point exceeds the threshold value κ_0, damage begins to evolve at that point. The function $\varepsilon_{eq} - \kappa_0 = 0$ is plotted in Figure 2 where κ_0 is set so that in uniaxial tension, damage will initiate when the cracking strain of concrete is exceeded. This means that for the particular case of uniaxial tension, the criterion $\varepsilon_{eq} - \kappa_0 = 0$ is the same as the Rankine criterion.

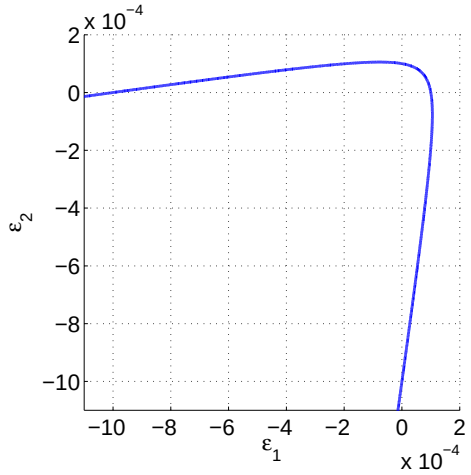

Figure 2: The function $\varepsilon_{eq} - \kappa_0 = 0$ in 2-D principal strain space

An important feature of the employed damage model is the non-local formulation achieved by considering also spatial gradients of the equivalent strain. Thus ill-posedness and mesh dependency that are typical in analysis of strain-softening materials (e.g. Bažant et al. [1984]) are avoided. The non-local equivalent strain denoted $\bar{\varepsilon}_{eq}$ is related to the local measure ε_{eq} by the partial differential equation

$$\bar{\varepsilon}_{eq} - c\nabla^2\bar{\varepsilon}_{eq} = \varepsilon_{eq} \tag{1}$$

where c is of the dimension length squared in 2-D and length cubed in 3-D. The complete derivation of Eq. (1) from the assumption that $\bar{\varepsilon}_{eq}$ represents a weighted average over a certain region is omitted for the purpose of brevity. We note that Eq. 1 is solved using a finite element discretization with the natural boundary conditions and can be conveniently coupled to the governing state equation of static equilibrium.

Applying the non-local approach, κ is determined at each material point according to the non-local equivalent strain $\bar{\varepsilon}_{eq}$ through the Karush-Kuhn-Tucker conditions

$$\dot{\kappa} \geq 0, \qquad \bar{\varepsilon}_{eq} - \kappa \leq 0, \qquad \dot{\kappa}(\bar{\varepsilon}_{eq} - \kappa) = 0$$

meaning that a) κ never decreases; b) κ 'registers' the extremal non-local equivalent strain; and c) when κ grows, then necessarily $\kappa = \bar{\varepsilon}_{eq}$.

The evolution of damage is represented as a process evolving in 'time', where the continuum problem (in the temporal sense) is transformed into a discrete one by applying an incrementation scheme. For every time increment, the weak form of the partial differential equilibrium equation is discretized using finite elements, leading to the force balance equation

$$\mathbf{f}^{u}_{ext} - \mathbf{f}^{u}_{int} = \mathbf{0}$$

where $\mathbf{f}^{u}_{ext}$ is the nodal external force vector accounting for volumetric, boundary and point loads. Similarly, the spatial discretization of Eq. (1) leads to

$$\mathbf{f}^{\varepsilon} - \mathbf{K}^{\varepsilon\varepsilon}\bar{\varepsilon}_{eq} = \mathbf{0}$$

Then the typical iterative system of equations to be solved by the Newton-Raphson method, with iterative displacements and non-local equivalent strains as unknowns at cycle i, is expressed as

$$\begin{bmatrix} \mathbf{K}^{uu}_{i-1} & \mathbf{K}^{u\varepsilon}_{i-1} \\ \mathbf{K}^{\varepsilon u}_{i-1} & \mathbf{K}^{\varepsilon\varepsilon} \end{bmatrix} \begin{bmatrix} \delta\mathbf{u}_i \\ \delta\bar{\varepsilon}_{eq,i} \end{bmatrix} = \begin{bmatrix} \mathbf{f}^{u}_{ext} \\ \mathbf{f}^{\varepsilon}_{i-1} \end{bmatrix} - \begin{bmatrix} \mathbf{f}^{u}_{int,i-1} \\ \mathbf{K}^{\varepsilon\varepsilon}\bar{\varepsilon}_{eq,i-1} \end{bmatrix} \tag{2}$$

where the incremental index is omitted for a clearer presentation. With the shape functions collected in $\mathbf{N}$ and $\tilde{\mathbf{N}}$ for the displacements and the non-local equivalent strains respectively (the shape functions are not necessarily of the same order); and with their derivatives collected in $\mathbf{B}$ and $\tilde{\mathbf{B}}$ respectively, the components of Eq. (2) are

$$\begin{aligned}
\mathbf{K}^{uu}_{i-1} &= \int_{\Omega} \mathbf{B}^T (1 - D_{i-1}) \mathbf{C}\mathbf{B} d\Omega \\
\mathbf{K}^{u\varepsilon}_{i-1} &= -\int_{\Omega} \mathbf{B}^T \mathbf{C} \varepsilon_{i-1} q_{i-1} \tilde{\mathbf{N}} d\Omega \\
\mathbf{K}^{\varepsilon u}_{i-1} &= -\int_{\Omega} \tilde{\mathbf{N}}^T \left(\frac{\partial \varepsilon_{eq}}{\partial \varepsilon} \right)^T_{i-1} \mathbf{B} d\Omega \\
\mathbf{K}^{\varepsilon\varepsilon} &= \int_{\Omega} \left(\tilde{\mathbf{N}}^T \tilde{\mathbf{N}} + \tilde{\mathbf{B}}^T c \tilde{\mathbf{B}} \right) d\Omega \\
\mathbf{f}^{u}_{int,i-1} &= \int_{\Omega} \mathbf{B}^T \sigma_{i-1} d\Omega \\
\mathbf{f}^{\varepsilon}_{i-1} &= \int_{\Omega} \tilde{\mathbf{N}}^T \varepsilon_{eq,i-1} d\Omega
\end{aligned}$$

Path-dependency enters the formulation through the scalar q which is non-zero only if κ (and therefore damage) is evolving with respect to the value at the previous converged increment denoted κ_{old}

$$q_{i-1} = \begin{cases} \left(\frac{\partial D}{\partial \kappa} \right)_{i-1} & \text{if} \quad \bar{\varepsilon}_{eq,i-1} > \kappa_{old} \\ 0 & \text{if} \quad \bar{\varepsilon}_{eq,i-1} \leq \kappa_{old} \end{cases}$$

In practice, a displacement-controlled incrementation is more suitable due to the strain-softening response. This means that a prescribed iterative displacement, denoted δu^p, is enforced at a particular degree of freedom (DOF). Then we have an unknown iterative load factor $\delta\theta$ instead of δu^p and the corresponding iterative equation system is slightly modified accordingly. In order to avoid modifying the tangent stiffness matrix (and for keeping its structure) we implement displacement control as suggested by Batoz and Dhatt [1979].

2.2 Embedded reinforcement formulation

A key component in the approach discussed in this article is the use of the embedded formulation for representation of rebars. The embedded formulation was initially suggested by Phillips and Zienkiewicz [1976] and later extended by Chang et al. [1987]. The main idea is that the stiffness of each individual rebar, modeled by a 1-D element, is added to the stiffness of the surrounding concrete domain, modeled by continuum elements. An example is sketched in Fig. 3. A single rebar is embedded into a hosting isoparametric 2-D element. It is assumed that the deformation of the bar is compatible to that of the hosting element. Therefore the strain in the bar is related to the element nodal displacements through the shape functions and its stiffness can be added at the element nodes.

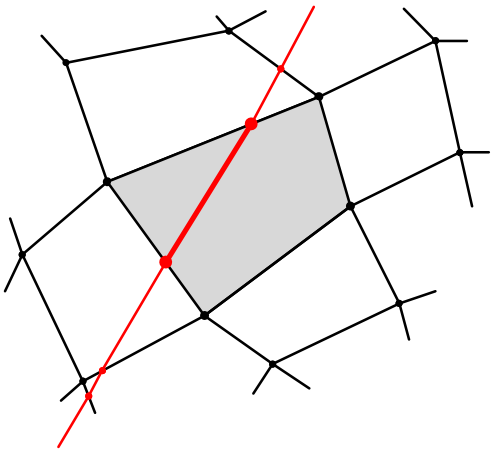

Figure 3: Example of a 1-D rebar embedded into an isoparametric 2-D element

In continuum-based topology optimization, the design domain is typically discretized using a structured grid mesh with equilateral elements. In truss topology optimization, a so-called 'ground structure' is constructed such that it consists of all possible connectivities of bars within the design domain. These practices make the embedded formulation very attractive because the complete truss ground structure can be embedded into the continuum grid in a relatively simple manner. Moreover, practical design requirements can be automatically considered due to the flexibility in the generation of the truss ground structure. Examples are physical spacing between bars; clear concrete cover with no reinforcement near the edges of the domain; and orthogonal reinforcement patterns (without diagonal bars) which are easier to construct. Demonstrative examples for truss structures embedded into a structured grid in 2-D are presented in Fig. 4.

The superposition of bar stiffnesses onto the hosting element stiffnesses is rather simple due to the way the ground structure is created. In essence, no element-level embedding is necessary because the truss elements share the same nodes as the hosting elements. This of course does not imply any loss of generality of the approach: the user may define bars in any location and embed them into the respective hosting elements. However, using a regularly-spaced truss structure with nodes that are compatible to those of the hosting mesh simplifies the embedding process by turning it into a global-level operation.

Finally, the contribution of the embedded truss structure to the global stiffness and internal force is added and Eq. (2) is modified accordingly

$$\begin{bmatrix} \mathbf{K}^{uu}_{i-1} + \mathbf{K}^{bars} & \mathbf{K}^{u\varepsilon}_{i-1} \\ \mathbf{K}^{\varepsilon u}_{i-1} & \mathbf{K}^{\varepsilon\varepsilon} \end{bmatrix} \begin{bmatrix} \delta \mathbf{u}_i \\ \delta \bar{\varepsilon}_{eq,i} \end{bmatrix} = \begin{bmatrix} \mathbf{f}^{u}_{ext} \\ \mathbf{f}^{\varepsilon}_{i-1} \end{bmatrix} - \begin{bmatrix} \mathbf{f}^{u}_{int,i-1} + \mathbf{f}^{bars}_{int} \\ \mathbf{K}^{\varepsilon\varepsilon} \bar{\varepsilon}_{eq,i-1} \end{bmatrix} \tag{3}$$

where $\mathbf{K}^{bars}$ and $\mathbf{f}^{bars}_{int}$ are the global stiffness matrix and internal forces corresponding to the complete set of truss bars. In the current study, the bars are considered as linear elastic.

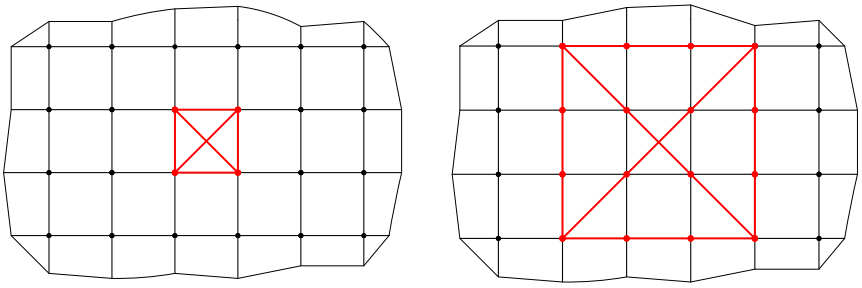

(a) The basic building block: truss bars embedded into a hosting square element

(b) A basic building block but with bigger physical spacing between bars

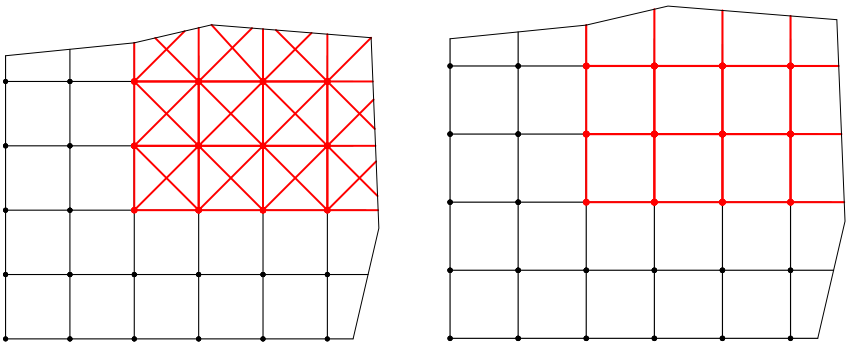

(c) Closely-spaced truss ground structure with clear cover near the edges

(d) Same as (c) but without diagonal bars

Figure 4: Demonstrative examples for truss structures embedded into a structured grid

3 Sensitivity analysis

In this section we provide some details regarding the sensitivity analysis procedure that should be carefully derived due to the nonlinearity and path-dependency of the structural analysis. In order to improve transparency in the presentation of the sensitivity analysis procedure, we artificially represent the structural analysis as a series of coupled equation systems corresponding to each of the 'time' increments. The first equation system is the global nonlinear incremental equilibrium that can be expressed as

$$\mathbf{R}_n(\mathbf{u}_n, \theta_n, \bar{\varepsilon}_{eq,n}, \kappa_{n-1}, \mathbf{x}) = \left[\begin{array}{c} \theta_n \hat{\mathbf{f}}^u_{ext} - \mathbf{f}^u_{int} \\ \mathbf{f}^\varepsilon - \mathbf{K}^{\varepsilon\varepsilon} \bar{\varepsilon}_{eq} \end{array} \right]_n = \mathbf{0}$$

where the unknowns at a certain increment n ($n = 1, ..., Nin$, Nin the number of increments) are the displacements $\mathbf{u}_n$, the load factor θ_n and the non-local equivalent strains $\bar{\varepsilon}_{eq,n}$; $\hat{\mathbf{f}}^u_{ext}$ is the constant reference load vector; κ_{n-1} are the history parameters at the previous converged step, on a gauss point level; and $\mathbf{x}$ is the vector of design variables. The second system is a collection of local equations which trace the path-dependencies throughout the evolution of damage

$$H_n(\bar{\varepsilon}_{eq,n}, \kappa_n, \kappa_{n-1}) = 0$$

At each point, two possible states exist

$$H_n = \left\{ \begin{array}{lll} \kappa_n - \bar{\varepsilon}_{eq,n} & \text{if} & \bar{\varepsilon}_{eq,n} > \kappa_{n-1} \\ \kappa_n - \kappa_{n-1} & \text{if} & \bar{\varepsilon}_{eq,n} \leq \kappa_{n-1} \end{array} \right.$$

where we note that $\bar{\varepsilon}_{eq,n}$, κ_n and κ_{n-1} are Gauss point quantities. The relation to the nodal quantities used above is given by $\bar{\varepsilon}_{eq,n} = \tilde{\mathbf{N}} \bar{\varepsilon}^e_{eq,n}$ where $\bar{\varepsilon}^e_{eq,n}$ are the nodal non-local equivalent strains in element e.

The representation of the structural analysis as a transient coupled problem enables utilization of the framework by [Michaleris et al., 1994] which in our opinion leads to a rather transparent and convenient adjoint sensitivity analysis procedure. For simplifying the presentation, we consider an objective functional related only to the final temporal state $\phi(\mathbf{x}) = G(\mathbf{u}_{Nin}(\mathbf{x}), \theta_{Nin}(\mathbf{x}), \bar{\varepsilon}_{eq,Nin}(\mathbf{x}), \kappa_{Nin-1}(\mathbf{x}), \mathbf{x})$ We begin by writing the augmented functional

$$\begin{aligned} \hat{\phi}(\mathbf{x}) \quad = \quad & G(\mathbf{u}_{Nin}(\mathbf{x}), \theta_{Nin}(\mathbf{x}), \bar{\varepsilon}_{eq,Nin}(\mathbf{x}), \kappa_{Nin-1}(\mathbf{x}), \mathbf{x}) \\ & - \sum_{n=1}^{Nin} \lambda_n^T \mathbf{R}_n(\mathbf{u}_n(\mathbf{x}), \theta_n(\mathbf{x}), \bar{\varepsilon}_{eq,n}(\mathbf{x}), \kappa_{n-1}(\mathbf{x}), \mathbf{x}) \\ & - \sum_{n=1}^{Nin-1} \sum_{gp=1}^{Ngp} \gamma_n H_n(\bar{\varepsilon}_{eq,n}(\mathbf{x}), \kappa_n(\mathbf{x}), \kappa_{n-1}(\mathbf{x})) \end{aligned}$$

where λ_n and γ_n are incremental adjoint vectors in the global and local level respectively; and Ngp is the number of Gauss points in the finite element. The design sensitivites with respect to a certain variable x_i are then obtained from the explicit derivatives of the augmented functional

$$\frac{\partial \phi}{\partial x_i} = \frac{\partial \hat{\phi}_{exp}}{\partial x_i} = \frac{\partial G}{\partial x_i} - \sum_{n=1}^{Nin} \lambda_n^T \frac{\partial \mathbf{R}_n}{\partial x_i} \tag{4}$$

The derivatives $\frac{\partial G}{\partial x_i}$ and $\frac{\partial \mathbf{R}_n}{\partial x_i}$ are related directly to the optimization problem and to the nonlinear model. The missing terms are the adjoint variables λ_n which are determined by requiring that all implicit derivatives of the augmented functional are eliminated.

In order to eliminate all implicit design sensitivities, a backwards-incremental adjoint procedure is performed. In the final increment denoted Nin, we aim to eliminate the implicit derivatives $\frac{\partial \mathbf{u}^f_{Nin}}{\partial \mathbf{x}}$, $\frac{\partial \theta_{Nin}}{\partial \mathbf{x}}$ and $\frac{\partial \bar{\varepsilon}_{eq,Nin}}{\partial \mathbf{x}}$ where the superscript f denotes non-prescribed (free) degrees of freedom. The resulting adjoint

equations are

$$\begin{aligned}
\left\{\frac{\partial G}{\partial \mathbf{u}^f_{Nin}}\right\} - \lambda^T_{Nin}\left[\frac{\partial \mathbf{R}_{Nin}}{\partial \mathbf{u}^f_{Nin}}\right] &= \mathbf{0} \\
\frac{\partial G}{\partial \theta_{Nin}} - \lambda^T_{Nin}\left\{\frac{\partial \mathbf{R}_{Nin}}{\partial \theta_{Nin}}\right\} &= 0 \\
\left\{\frac{\partial G}{\partial \bar{\varepsilon}_{eq,Nin}}\right\} - \lambda^T_{Nin}\left[\frac{\partial \mathbf{R}_{Nin}}{\partial \bar{\varepsilon}_{eq,Nin}}\right] &= \mathbf{0}
\end{aligned} \tag{5}$$

Note that the expressions $-\frac{\partial \mathbf{R}_{Nin}}{\partial \mathbf{u}^f_{Nin}}$ and $-\frac{\partial \mathbf{R}_{Nin}}{\partial \bar{\varepsilon}_{eq,Nin}}$ are the components of the non-prescribed DOF in the tangent stiffness matrix $\mathbf{K}_{Nin}$ corresponding to the converged state at increment Nin. Therefore the adjoint system (5) can be solved using a similar stiffness matrix $\tilde{\mathbf{K}}_{Nin}$ that is the same as $\mathbf{K}_{Nin}$ except for a modification of the column denoted by the superscript p corresponding to the prescribed DOF

$$\begin{aligned}
\tilde{\mathbf{K}}^f_{Nin} &= \mathbf{K}^f_{Nin} \\
\tilde{\mathbf{K}}^p_{Nin} &= \frac{\partial \mathbf{R}_{Nin}}{\partial \theta_{Nin}}
\end{aligned}$$

Finally the linear system to be solved is

$$\tilde{\mathbf{K}}^T_{Nin}\lambda_{Nin} = \left\{\begin{array}{c} -\left\{\frac{\partial G}{\partial \mathbf{u}^f_{Nin}}\right\}^T \\ \frac{\partial G}{\partial \theta_{Nin}} \\ -\left\{\frac{\partial G}{\partial \bar{\varepsilon}_{eq,Nin}}\right\}^T \end{array}\right\} \tag{6}$$

Stepping backwards to increment $Nin-1$, we aim to eliminate the implicit derivatives $\frac{\partial \kappa_{Nin-1}}{\partial \mathbf{x}}$. This is achieved by setting the local adjoint variables

$$\gamma_{Nin-1} = \frac{\partial G}{\partial \kappa_{Nin-1}} - \left\{\frac{\partial \mathbf{R}_{Nin}}{\partial \kappa_{Nin-1}}\right\}^T \lambda_{Nin}$$

where the equality $\frac{\partial H_{Nin-1}}{\partial \kappa_{Nin-1}} = 1$ was utilized. The derivative $\frac{\partial \mathbf{R}_{Nin}}{\partial \kappa_{Nin-1}}$ is non-zero only in points where path-dependency occurs at increment Nin, meaning damage was determined by κ_{Nin-1} rather than by $\bar{\varepsilon}_{eq,Nin}$. From here a general form for the global adjoint equation that holds for increments $n = 1,...,Nin-1$ is revealed. It is the same as Eq. (5) but has no derivatives of G and has an additional right-hand-side term involving γ_n which introduces the path-dependency

$$\begin{aligned}
-\lambda^T_n\left[\frac{\partial \mathbf{R}_n}{\partial \mathbf{u}^f_n}\right] &= \mathbf{0} \\
-\lambda^T_n\left\{\frac{\partial \mathbf{R}_n}{\partial \theta_n}\right\} &= 0 \\
-\left\{\gamma_n \frac{\partial H_n}{\partial \bar{\varepsilon}_{eq,n}}\tilde{\mathbf{N}}\right\} - \lambda^T_n\left[\frac{\partial \mathbf{R}_n}{\partial \bar{\varepsilon}_{eq,n}}\right] &= \mathbf{0}
\end{aligned}$$

This means that the added term to the right-hand-side is an assembly onto the global level of local terms corresponding to points where $\frac{\partial H_n}{\partial \bar{\varepsilon}_{eq,n}}$ is non-zero. Then the linear system to be solved in the general increment is

$$\tilde{\mathbf{K}}^T_n\lambda_n = \left\{\begin{array}{c} \mathbf{0} \\ 0 \\ \left\{\tilde{\mathbf{N}}^T \frac{\partial H_n}{\partial \bar{\varepsilon}_{eq,n}}\gamma_n\right\} \end{array}\right\} \tag{7}$$

Finally, the general form for the expression used to compute the local adjoints, that holds for increments $n = 1, ..., Nin - 2$ is revealed as

$$\gamma_n = -\left\{ \frac{\partial \mathbf{R}_{n+1}}{\partial \kappa_n} \right\}^T \lambda_{n+1} - \frac{\partial H_{n+1}}{\partial \kappa_n} \gamma_{n+1} \tag{8}$$

In summary, the backwards-incremental adjoint procedure consists of the following steps:

1. Solve for λ_{Nin} using Eq. (6).
2. Collect design sensitivities according to Eq. (4).
3. Set for all Gauss points $\gamma_{Nin} = 0$.
4. Repeat for $n = Nin - 1, ..., 1$:
   (a) For all Gauss points compute γ_n using Eq. (8) and assemble extra term of right-hand-side for Eq. (7).
   (b) Solve for λ_n using Eq. (7).
   (c) Collect design sensitivities according to Eq. (4).

Concluding this section, we note that the computed design sensitivities were found to be in perfect agreement with numerical derivatives based on finite differences.

4 Topology optimization

The aim is to distribute a given volume of steel reinforcement bars within a certain concrete domain so that the stiffest structure is obtained. In the case of a nonlinear structural response and a displacement-controlled analysis, this can be posed as maximization of the end-compliance. In other words, we seek to maximize the load-bearing capacity in the final equilibrium state corresponding to the desired value of the total prescribed displacement.

4.1 Design parametrization

The approach for obtaining an optimized layout of reinforcement bars follows common truss optimization procedures based on the ground structure approach (see for example Bendsøe and Sigmund [2003] for an overview of this method). The cross-section area of each bar element in the truss ground structure is associated to a design variable. In general, we consider zero bar areas to be feasible so the optimization problem combines topology and sizing.

The relation between a certain bar area in element i and the corresponding mathematical design variable is given by a linear interpolation

$$a_i = a_{min} + (a_{max} - a_{min}) x_i$$

where a_i is the physical cross-section area; a_{min} and a_{max} are lower and upper bounds of the desired range of areas; and x_i is the design variable, $0 \leq x_i \leq 1$. The choice of a_{min} and a_{max} gives the user control over the outcome of optimization and should be related to the actual purpose of employing structural optimization. For example, if we seek only qualitative insight regarding the optimal distribution of reinforcement, we may define $a_{min} = 0$ and set a_{max} so that it corresponds to the available volume and to the geometry of the domain. On the other hand, if we wish to generate a practical reinforcement layout, then a_{min} may correspond to minimal reinforcement requirements provided the ground structure represents a manufacturable rebar pattern. Furthermore, a_{max} can be related to the maximum bar area we would like to use in construction.

Another parameter that should be chosen in accordance with the desired outcome is the degree of penalization. We employ a modified SIMP [Bendsøe, 1989, Sigmund and Torquato, 1997] interpolation scheme so that the stiffness matrix of bar i is given by

$$\mathbf{K}_i = E_{steel}(a_{min} + (a_{max} - a_{min})x_i^{p_{bar}})\mathbf{K}_i^0 \tag{9}$$

where $p_{bar} \geq 1$ is the penalization factor and $\mathbf{K}_i^0$ is a parametric stiffness matrix of the bar for $E = 1$, $a = 1$. In principle, the most freedom is given to the optimization procedure when no penalization is considered ($p_{bar} = 1$). The result in terms of continuously varying bar areas can then be post-processed to fit available bar types in practice. Nevertheless, one may consider adding penalization ($p_{bar} > 1$) for various purposes. Examples are to approach a 0-1 design with a single bar type; or to obtain a 'clean' layout with realistic physical spacing between bars when the ground structure is relatively dense.

4.2 Problem formulation

With the parametrization described above, the optimization problem to be solved is expressed as

$$\begin{aligned} \min_{\mathbf{x}} \phi \quad &= \quad -\theta_{Nin}\hat{f}^p u_{Nin}^p \\ \text{s.t.:} \quad & \sum_{i=1}^{N_{bars}} a_i l_i \leq \rho V \\ & 0 \leq x_i \leq 1, \qquad i = 1,...,N_{bars} \\ \text{with:} \quad & \mathbf{R}_n(\mathbf{u}_n, \theta_n, \bar{\varepsilon}_{eq,n}, \kappa_{n-1}, \mathbf{x}) = 0 \qquad n = 1,...,Nin \\ & \mathbf{H}_n(\bar{\varepsilon}_{eq,n}, \kappa_n, \kappa_{n-1}) = 0 \qquad n = 1,...,Nin-1 \end{aligned} \tag{10}$$

where N_{bars} is the number of bars in the ground structure; l_i is the length of bar i; ρ is the reinforcement volume ratio; and V is the volume of the concrete domain.

The compliance measure takes into account only the prescribed DOF even though a general distributed load is considered. Maximizing the complete end-compliance $\theta_{Nin}\hat{\mathbf{f}}^T\mathbf{u}_{Nin}$ does not necessarily lead to the stiffest structural layout: because the displacement is prescribed at a single DOF while the same load factor θ multiplies all nodal loads, maximizing $\theta_{Nin}\hat{\mathbf{f}}^T\mathbf{u}_{Nin}$ may result in a structure that is very stiff with respect to bearing the load at the prescribed DOF but very flexible with respect to all other loads. In the current study, we only consider concentrated loads that are distributed locally in the vicinity of the prescribed DOF so that a better finite element approximation is obtained. Optimizing for general distributed loads with a displacement-controlled nonlinear analysis requires the definition of a suitable objective functional for obtaining 'the stiffest structure'. A certain intuitive remedy for this in the form of a hybrid procedure, using a load-controlled objective and a displacement-controlled analysis, was proposed and applied by Bogomonly and Amir [2012]. However, it appears to be applicable only in cases where the force-displacement relation is unique.

4.3 Particular sensitivity analysis

With respect to the general sensitivity analysis procedure described in Section 3, the only non-zero derivative of the paricular objective in (10) is $\frac{\partial G}{\partial \theta_{Nin}} = -\hat{f}^p u_{Nin}^p$ that enters Eqs. (5) and (6). The adjoint equation system corresponding to the final increment is therefore

$$\tilde{\mathbf{K}}_{Nin}^T \lambda_{Nin} = \left\{ \begin{array}{c} \mathbf{0} \\ -\hat{f}^p u_{Nin}^p \\ \mathbf{0} \end{array} \right\}$$

Furthermore, the derivative $\frac{\partial \mathbf{R}_n}{\partial x_i}$ in Eq. (4) involves only bar forces and is easily evaluated for each design variable as follows

$$\frac{\partial \mathbf{R}_n}{\partial x_i} = -p_{bar} x_i^{(p_{bar}-1)}(a_{max} - a_{min})E_{steel}\mathbf{K}_i^0 \mathbf{u}_{n,i}$$

where $\mathbf{u}_{n,i}$ are the displacements computed at increment n in the $i-$th element's degrees of freedom.

4.4 Case study: 2-D deep beam

In this section, we demonstrate the application of the proposed approach to reinforcement design of a 2-D deep beam. The problem setting and the computational model for analysis and optimization are described in Figure 5. This is a rather simple case from the design point of view so attention can be focused on investigating the influence of the various parameters on the outcome of optimization.

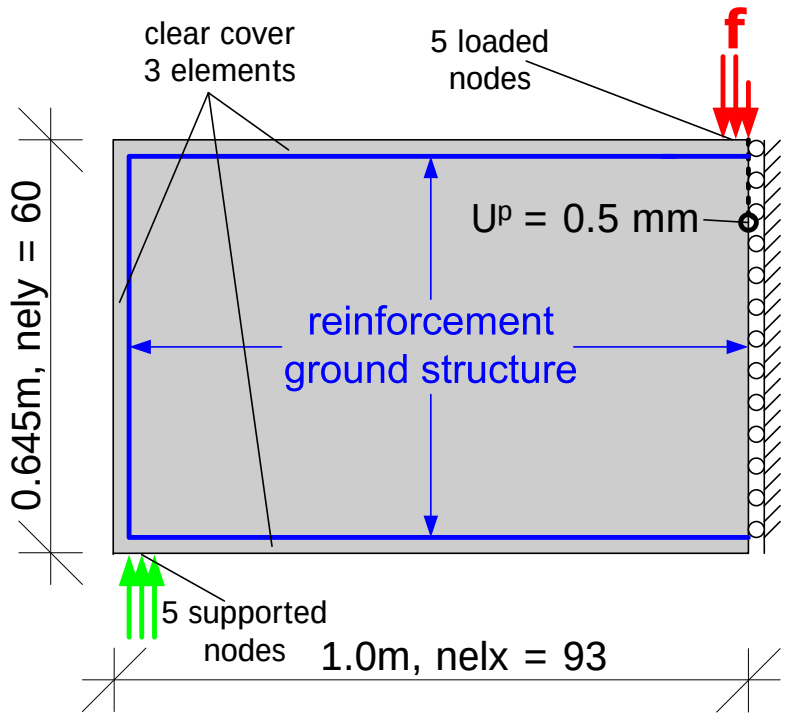

Figure 5: Problem setting and computational model, symmetric half of a 2-D deep beam

Ground structures Three different ground structures are utilized in this case study, as presented in Figure 6. The first, denoted GS1, consists of basic building blocks (see Figure 4) over the entire continuum mesh, excluding the clear cover regions. The second, denoted GS2, consists of the same type of building blocks but with larger (and more practical) spacing, corresponding to roughly 0.1m between bars in the x and y directions. The third ground structure, denoted GS3, is the same as the second but with bars only in Cartesian directions, which is typically preferable due to easier construction. There exist of course many other possibilities of defining the acceptable positions of reinforcement bars. Nevertheless, we believe that these three particular variants demonstrate the freedom and control given to the designer in the setup of the optimization problem.

Comparison to linear-elastic optimization We first wish to benchmark the results obtained by the proposed procedure against two other optimization procedures based on linear-elastic analysis. We compare the performance of three optimized layouts generated as follows:

1. **Linear-elastic truss optimization**. In this approach, concrete is absent so the load is carried by the truss structure which is optimized to achieve minimum compliance for a fixed load. This is essentially the idea of generating a strut-and-tie model by topology optimization, but with a truss ground structure as suggested by Moen and Guest [2010]. In the next step, it is assumed that only the tensile bars in this optimized truss represent the reinforcement layout. The tensile bar areas are then scaled so that the total volume of reinforcement is the same as for the other cases.

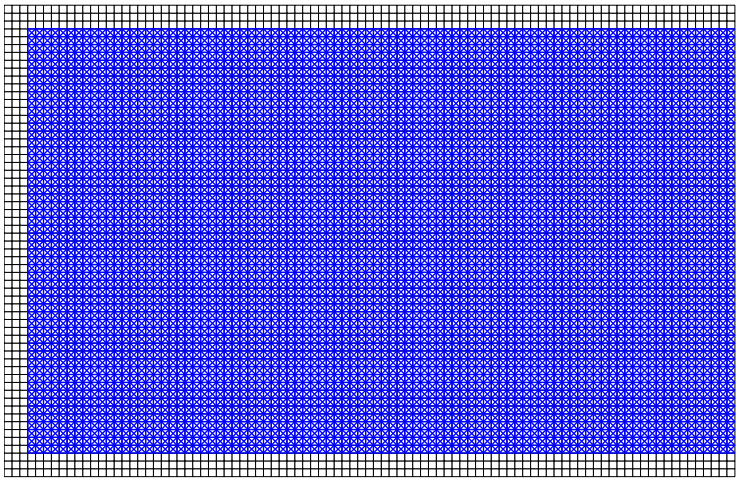

(a) Ground structure 1 (GS1): densely-spaced truss structure

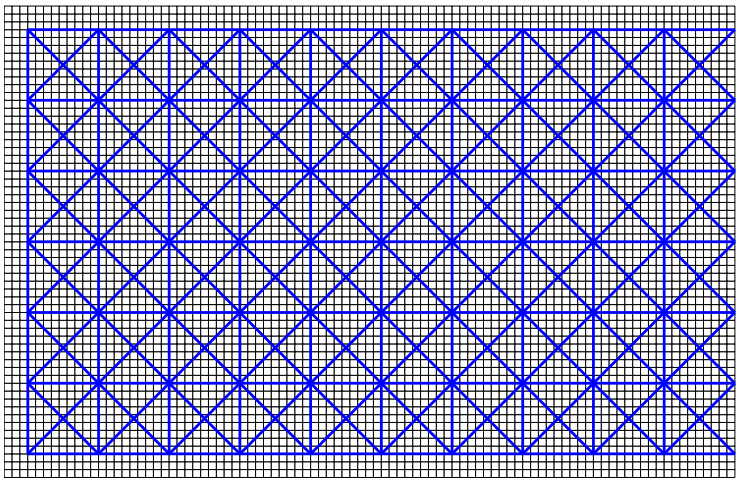

(b) Ground structure 2 (GS2): sparsely-spaced truss structure with 9×9 element modules

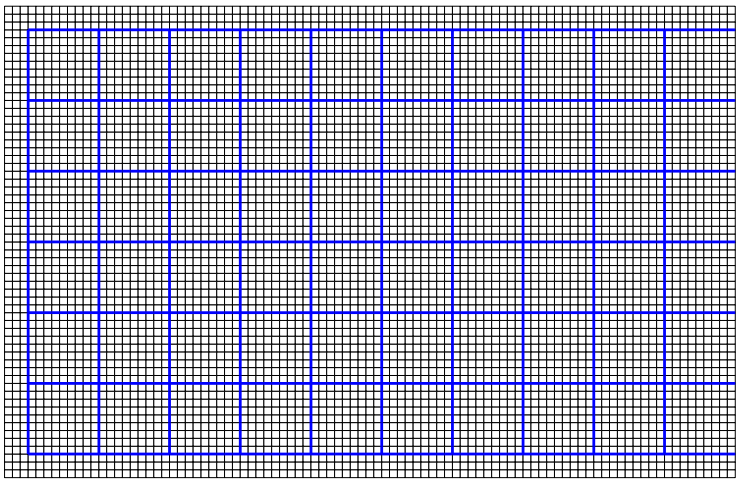

(c) Ground structure 3 (GS3): same as (b) but without diagonal bars

Figure 6: Three variants of truss ground structures for the deep beam example, symmetric half

2. **Linear-elastic embedded rebar optimization**. This approach is the same as proposed in this article but without the nonlinear material modeling. Both tension and compression in rebars are acceptable as opposed to a strut-and-tie force transfer mechanism.

3. **Damage-based embedded rebar optimization**. This is the procedure suggested in this article where the distribution of embedded rebars is optimized considering damage in the hosting concrete.

The three structures are evaluated considering damage with the suggested respective reinforcements.

For this comparison, GS2 was utilized along with the following parameters: reinforcement ratio $\rho = 0.005$; de-localization parameter $c = (l_y/10)^2$ (=0.0042m^2); $a_{min} = 1 \times 10^{-10}$ (=1×10^{-4}mm^2/m); $a_{max} = \rho\sqrt{V}$ (=4016mm^2/m); and $p_{bar} = 1$. The damage-based optimization converged after 92 iterations, when the change in all design variables did not exceed 1×10^{-6}. The resulting objective values ϕ, equal to minus the end-compliance, are -3.3561×10^{-5} for the linear-elastic truss optimization; -3.4453×10^{-5} for the linear-elastic embedded rebar optimization; and -3.5486×10^{-5} for the damage-based optimization. With respect to a reference value of -2.9612×10^{-5} corresponding to an initial uniform distribution of reinforcement, the damage-based truss optimization gives nearly 50% extra improvement in objective value over the linear-elastic truss optimization and more than 20% extra improvement over the linear-elastic embedded procedure. This justifies the utilization of a more elaborate model despite the higher computational demands. In future applications we intend to consider also objectives involving control of damage or cracking, where the benefit of nonlinear material modeling should be even more significant.

The difference between the linear-elastic and the damage-based approaches can be clarified by examining the optimized layouts, see Figure 7. In the damage-based optimization, rebars are mainly distributed where the structure is severely damaged, namely in the bottom fibers. Some reinforcement is also positioned in the vicinity of the concentrated load so that damage is avoided there. In the linear-elastic embedded approach the same regions are reinforced but without preference to the tensile state due to the absence of failure. The linear-elastic truss optimization assumes that the tensile forces are transferred through truss bars only and thus does not account for the contribution of the undamaged concrete. In other words, linear-elastic optimization may be used to generate a valid strut-and-tie model but this will not necessarily give the optimal distribution of reinforcement.

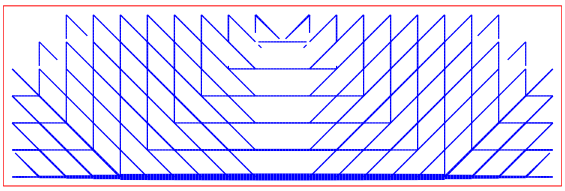

(a) Tensile rebars only according to a linear-elastic truss optimization, $\phi = -3.3561 \times 10^{-5}$

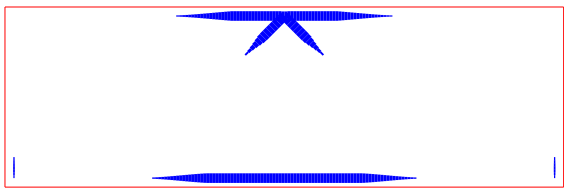

(b) Distribution of rebars according to a linear-elastic embedded rebar optimization, $\phi = -3.4453 \times 10^{-5}$

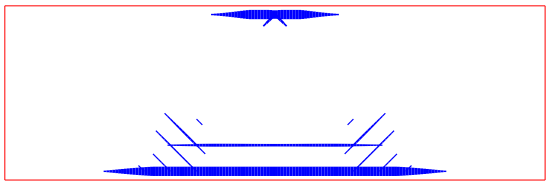

(c) Distribution of rebars according to a damage-based embedded rebar optimization, $\phi = -3.5486 \times 10^{-5}$

Figure 7: Deep beam case study: comparison of optimized layouts for different optimization approaches with GS2.

For further comparisons aimed at examining the effect of the various parameters, the result obtained with damage-based optimization and presented in Figure 7(c) is used as reference. By varying one parameter at a time, we will try to provide insight regarding the sensitivity of the proposed procedure to the choice of ground structure, penalty factor and de-localization parameter.

Effect of ground structure resolution We now focus on how the choice of the ground structure influences the outcome of optimization. We use the three variants GS1, GS2 and GS3 mentioned above; all other parameters are kept the same as for the previous comparison. The optimized layouts obtained with GS1 and GS3 are shown in Figure 8 while the result with GS2 was already shown in Figure 7(c). The objective values are -3.5714×10^{-5} and -3.5474×10^{-5} respectively. As expected, a larger variety of rebars in the ground structure leads to a better result: $\phi_{\text{GS1}} < \phi_{\text{GS2}} < \phi_{\text{GS3}}$. However, the layout generated with GS1 consists of a very dense distribution of diagonal rebars; this poses a problem for automatic post-processing of a reinforcement plan. As will be discussed in the next section, penalization can be applied for 'cleaning' such layouts.

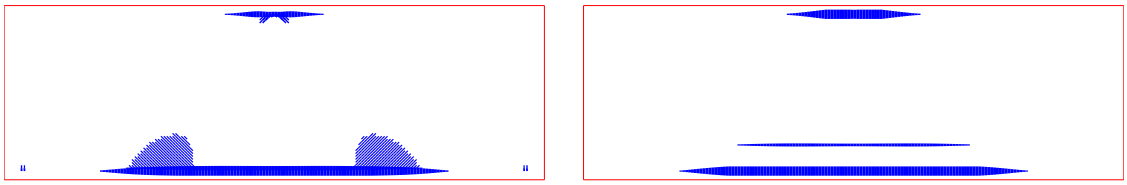

(a) Optimized layout with GS1, $\phi = -3.5714 \times 10^{-5}$ (b) Optimized layout with GS3, $\phi = -3.5474 \times 10^{-5}$

Figure 8: Deep beam case study: effect of different ground structures

Effect of penalty factor According to various numerical experiments conducted in this study, the optimization procedure easily converges towards distinct layouts without applying any penalization of intermediate densities. If continuous cross-section areas are acceptable as a result of optimization, then in principle no penalization is necessary. Nevertheless, when using very dense ground structures the final layout consists of closely-spaced rebars and one may want to obtain a cleaner design prior to the generation of an actual reinforcement plan. Mild penalization can be successfully utilized for this purpose, as demonstrated in Figure 9. We note that in the presented layouts, the horizontal bar in the bottom fiber typically consists of multiple layers which seem merged due to the linear relation between the bar area and the plotted line width. This is clarified by the 'zoom-in' in Figure 9(d).

Using the dense GS1, we gradually raise p_{bar} from 1.00 to 1.05. It can be seen that the dense diagonal bars are gradually eliminated. This comes with little compromise on the performance of the structure: the objective value corresponding to the optimized design with GS1 and $p_{bar} = 1.00$ was -3.5714×10^{-5}; the objective value corresponding to the design obtained with gradual penalization was -3.5704×10^{-5} (evaluated with the physical $p_{bar} = 1.00$). This highlights a clear tendency to use as much material as possible for bars positioned as close as possible to the bottom fiber, whereas diagonal bars resisting shear cracking are less significant for the compliance objective.

Effect of de-localization parameter The de-localization parameter c in Eq. (1) determines the size of the averaging domain in the nonlocal damage model and therefore introduces a length scale in the solution of the state equations. In general, small values of c lead to a more localized response along with more extensive damage. High values of c cause the damage to spread smoothly over a larger area (or volume) and thus the extremal degree of damage is reduced. It is difficult to state an ideal value of c, but from the optimization perspective c should correspond to the geometry of the concrete domain and to the spacing of the rebars. The impact on the optimized layouts can be observed in Figure 10 where both the damage distribution and the layout are presented side-by-side for the symmetric half. The layout can be compared to the reference design in Figure 7(c). The length scale introduced by the parameter c clearly affects the rebar distribution: the presence of a certain rebar contributes to the reduction of damage in its close neighborhood, which is defined by c. Therefore smaller values of c require a finer distribution of rebars, whereas enlarging the averaging domain leads to more 'concentrated' rebar distributions.

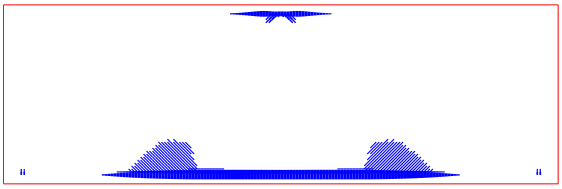

(a) After 50 design iterations, $p_{bar} = 1.000$

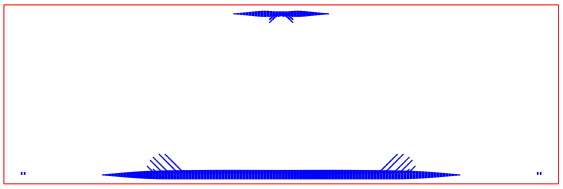

(b) After 50 further design iterations, $p_{bar} = 1.025$

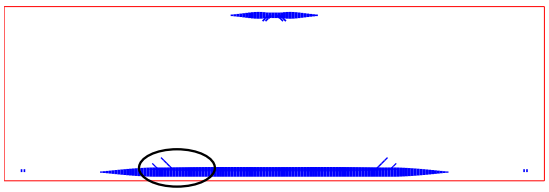

(c) After 50 further design iterations, $p_{bar} = 1.050$

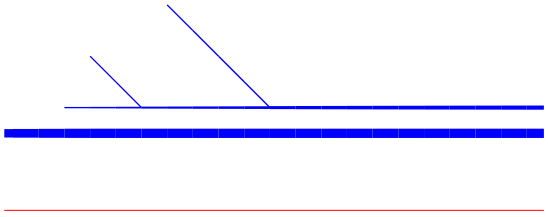

(d) Focus on particular region in the final layout

Figure 9: Deep beam case study: effect of added penalization

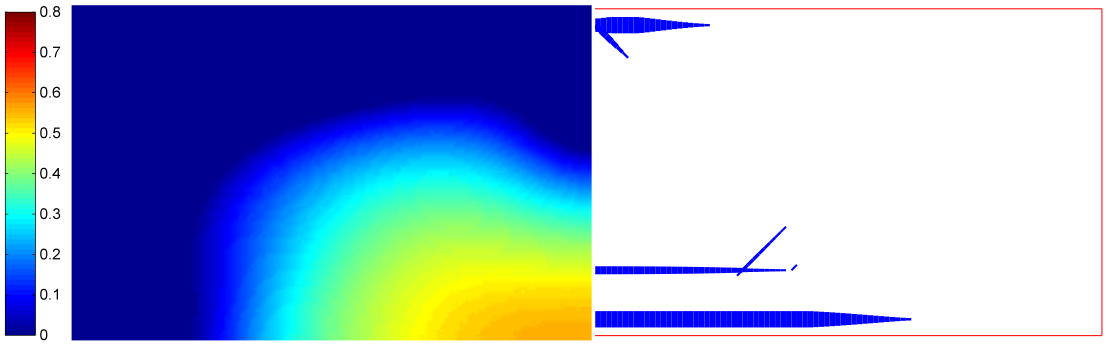

(a) Damage and optimized layout with $c = (l_y/5)^2$ (=0.0166m^2), $\phi = -3.6941 \times 10^{-5}$

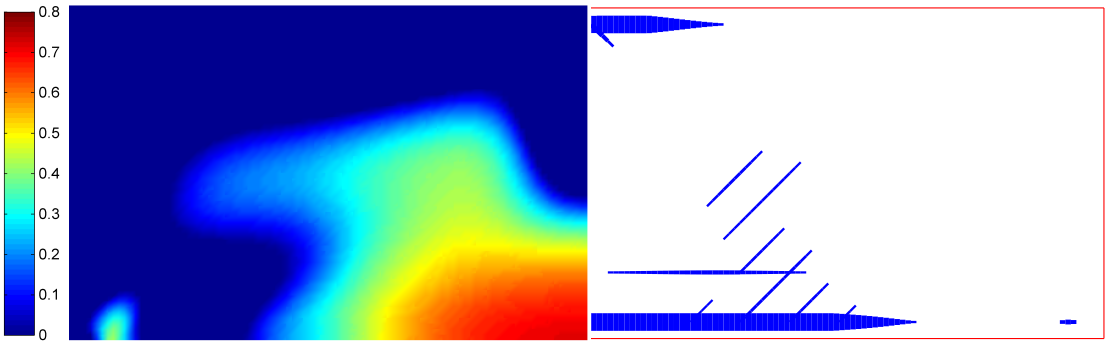

(b) Damage and optimized layout with $c = (l_y/20)^2$ (=0.0010m^2), $\phi = -3.4682 \times 10^{-5}$

Figure 10: Deep beam case study: effect of de-localization parameter

Table 1: Material properties used in all examples

E_c [MPa]	ν	κ_0	m	α	β	E_s [MPa]
30,000	0.2	1.818×10^{-4}	0.818	0.95	100	200,000

Table 2: Dimensions of reinforcement bars

Diameter [mm]	Area [mm^2]	a_{max} [m^2/m]
16	201	2.011×10^{-3}
18	254	2.545×10^{-3}
20	314	3.142×10^{-3}
22	380	3.801×10^{-3}
25	491	4.909×10^{-3}

5 Examples

Several examples of reinforcement layouts are presented in this section. The focus is on load-bearing concrete structures, where self-weight is insignificant with comparison to the external load. The loads are in principle point forces which are distributed locally in order to avoid artificial stress concentrations due to the finite element discretization. A small prescribed displacement is imposed at the central loading point and the analysis is performed using displacement control with adaptive incrementation. In the examples presented, the number of increments was usually between 6 to 10 and the number of Newton-Raphson iterations per increment between 1 to 5. For two-dimensional problems, the continuum mesh for concrete consists of square, 4-node plane stress elements. For three-dimensional problems, 8-node cube elements are utilized. Material properties are kept constant for all examples and are given in Table 1. The only exception is the de-localization parameter which is set according to the particular geometry. The procedure is implemented in FORTRAN and the optimization is performed by the Method of Moving Asymptotes - MMA [Svanberg, 1987]. The optimization is terminated when the biggest absolute change in the values of the design variables is smaller than 1×10^{-6}; if this criterion is not met, then typically a maximum of 100 design cycles are performed. According to the authors' experience, only small changes occur after 30 design cycles and after 100 cycles the maximum absolute change seldom exceeds 1×10^{-4}.

An important parameter whose influence is examined in the following examples is the value of a_{max}. In order to achieve results close as possible to practical reinforcement plans, we choose various values of a_{max} according to typical bar types used in the construction industry. A list of five bar types and the corresponding values for the design parametrization (9) is given in Table 2. In two-dimensional cases, it is assumed that the bars are positioned every 0.1m in the thickness direction. Therefore the value of a_{max} corresponds to the area of 10 rebars per unit thickness.

5.1 2-D corbel

We consider the design of a 2-D corbel, which was previously examined by several researchers in the context of applying continuum topology optimization for generating strut-and-tie models [Kwak and Noh, 2006, Bruggi, 2009, Victoria et al., 2011]. The setting of the problem is given in Figure 11, including details regarding the finite element discretization and the position of the truss ground structure. Two types of ground structures are utilized which are equivalent to the types GS2 and GS3 described above, with a spacing of 6 continuum elements between adjacent bar elements. The parameter c for the nonlocal damage formulation is set to 0.0025 m^2 and the volume of steel is set to $0.005 \times V$ in all simulations.

First we examine the results obtained with $a_{min} = 0$. The optimized layouts can be observed in Figure 12. The influence of the parameter a_{max} is clear: for maximizing the end-compliance, it is beneficial to place as much material as possible in a few critical bar positions. If a lower a_{max} is imposed, then rebars are more widely distributed in the domain but the performance is compromised. Furthermore, it can be seen that

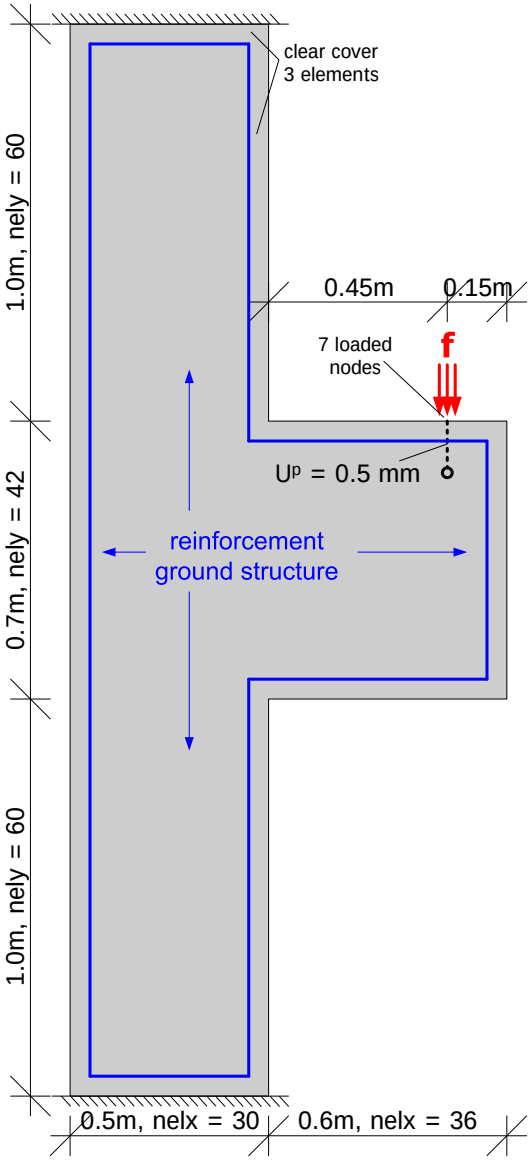

Figure 11: 2-D corbel: problem setting and computational model

for the compliance objective in the prescribed range of deformation, it is sometimes better to allow limited tension in the concrete while reinforcing compression regions. This can be seen especially in the result with GS3 and a_{max} = 2011mm^2/m, where the upper part of the column acts mainly in tension and is not reinforced, while some rebars are placed in the lower part of the column and act in compression. In principle, a strut-and-tie model will predict a different distribution, because it assumes that the concrete phase is completely cracked in tension.

As mentioned above, the parameter a_{min} can be utilized to introduce a minimal reinforcement distributed uniformly throughout the truss ground structure. In Figure 13 we present the layout obtained for the same problem setting with GS3, but with a_{min} = 1131mm^2/m and a_{max} = 4909mm^2/m. The result is in principal very similar to that obtained with a_{min} = 0 and a_{max} = 4909mm^2/m, in the sense that the thick rebars are positioned in the same locations. However, it is expected that adding minimal reinforcement will reduce the concrete crack widths in the regions of tensile stresses. For practical applications, we note that the designer is free to define any minimal reinforcement pattern and embed it within the concrete domain. The corresponding rebars will not be related to the design variables in the optimization problem, which will determine only the layout of the *additional* reinforcement.

5.2 2-D wall with opening

In this example we aim at designing the reinforcement for a wall with an opening, see Figure 14 for the problem setting. Schlaich et al. [1987] gave it thorough consideration when demonstrating the strut-and-tie modeling approach for design of structural concrete. It was also used as an example for applying continuum topology optimization as a means of generating strut-and-tie models, initially by Liang et al. [2000] and later by other investigators [Kwak and Noh, 2006, Bruggi, 2009, Victoria et al., 2011]. Two types of ground structures are utilized: both use a grid with the same spacing as the continuum grid, with or without diagonal bars. The parameter c for the nonlocal damage formulation is set to $c = (l_y/15)^2$ (=0.0982 m^2) in all simulations. The volume of steel is set to $0.005 \times V$; a_{max} = 4909mm^2/m and a_{min} is zero.

In order to eliminate dense distributions of thin bars, penalization is introduced gradually: we perform three stages of 50 design iterations, with the values of $p_{bar} = 1.00$, $p_{bar} = 1.25$ and $p_{bar} = 1.50$ respectively. The resulting layouts presented in Figures 15 and 16 demonstrate the significance of the ground structure layout. While the response of the concrete phase in both structures is similar as can be observed in the principal stress plots, the contribution of reinforcement is fundamentally different. When diagonal rebars are available, they are used primarily to reinforce the shear block on the right side of the structure where rebars act both in tension as well as in compression. According to the reaction forces, this shear block carries roughly 2/3 of the load in both cases; therefore the stiffening due to reinforcement is favorable for improving the load-bearing capacity. Examining the objective values, using diagonal reinforcement leads to 30.3% improvement compared to the initial design, while without diagonals only 15.4% is achieved. The structure with diagonals has an overall lower level of damage, in particular within the shear block. At the same time, the absence of massive reinforcement in the bottom fiber causes higher levels of damage there, compared to the structure without diagonals.

5.3 3-D pile cap

As a final example we consider the rebar distribution in a pile cap which is essentially a three-dimensional box-shaped block, see Figure 17 for the problem setting, the initial design and the resulting layout. The pile cap transfers a vertical force from a column (or bridge pier) to four piles positioned in a rectangular layout. Double symmetry is exploited so only one quarter of the pile cap is modeled and optimized. The ground structure is a simple 3-D extension of GS1 with a clear cover of one finite element in all directions excluding symmetry planes. The parameter c for the nonlocal damage formulation is set to $c = (l_y/5)^3$ (=0.001 m^3). The volume of steel is set to $0.005 \times V$; a_{max} = 4909mm^2/m and a_{min} is zero.

In this example we again introduce gradual penalization in three stages of 50 design iterations with $p_{bar} = 1.00$, $p_{bar} = 1.25$ and $p_{bar} = 1.50$. In the optimized layout, rebars are mainly positioned in the bottom fiber in the direction of the major bending action; as well as right above the piles where strong reaction forces

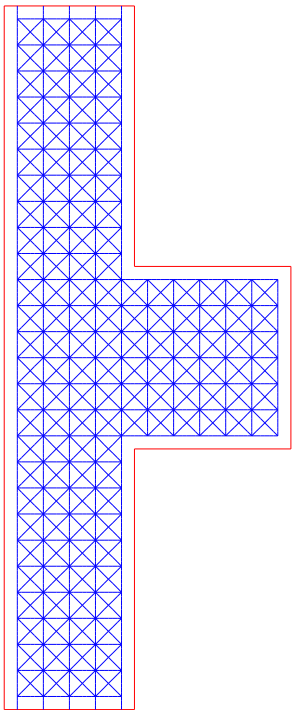

(a) GS2 with uniform distribution of reinforcement, $\phi = -6.171 \times 10^{-5}$

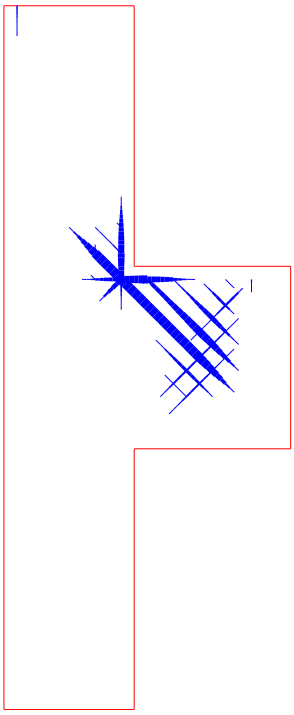

(b) Optimized layout with GS2 and a_{max} = 4909mm^2/m, $\phi = -7.462 \times 10^{-5}$

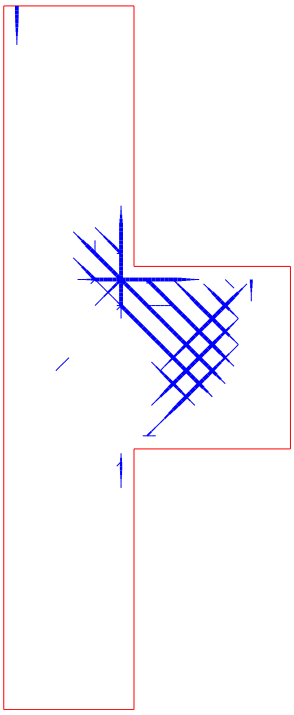

(c) Optimized layout with GS2 and a_{max} = 2011mm^2/m, $\phi = -7.292 \times 10^{-5}$

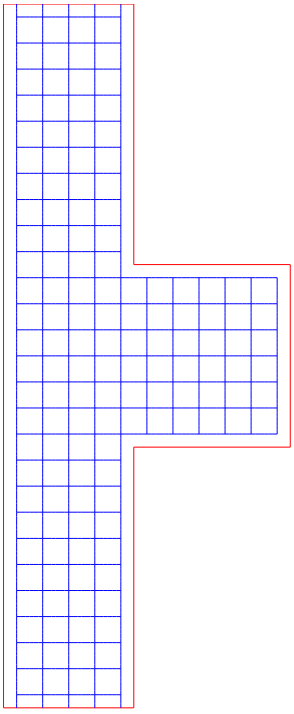

(d) GS3 with uniform distribution of reinforcement, $\phi = -6.062 \times 10^{-5}$

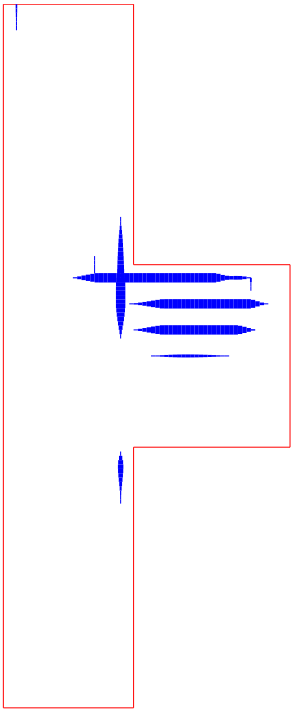

(e) Optimized layout with GS3 and a_{max} = 4909mm^2/m, $\phi = -6.504 \times 10^{-5}$

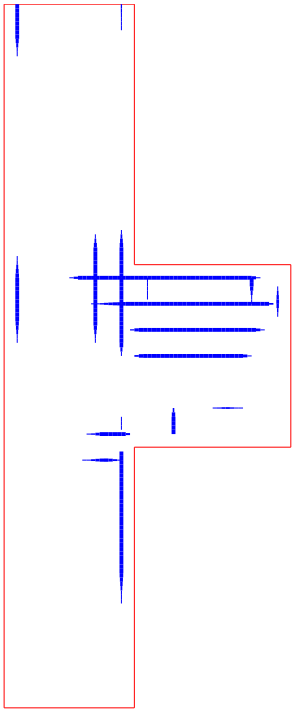

(f) Optimized layout with GS3 and a_{max} = 2011mm^2/m, $\phi = -6.353 \times 10^{-5}$

Figure 12: Reinforcement layouts for the 2-D corbel

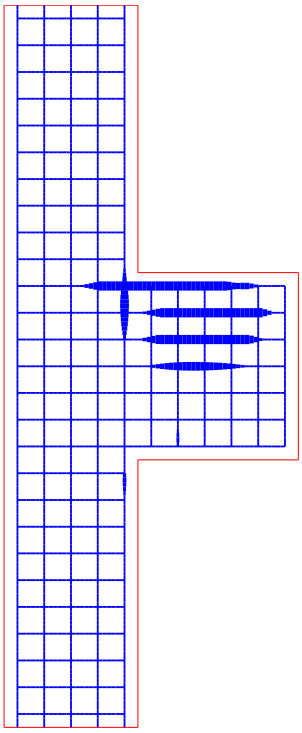

Figure 13: Reinforcement layout for the 2-D corbel: optimized layout with GS3, a_{min} = 1131mm^2/m and a_{max} = 4909mm^2/m, $\phi = -6.481 \times 10^{-5}$

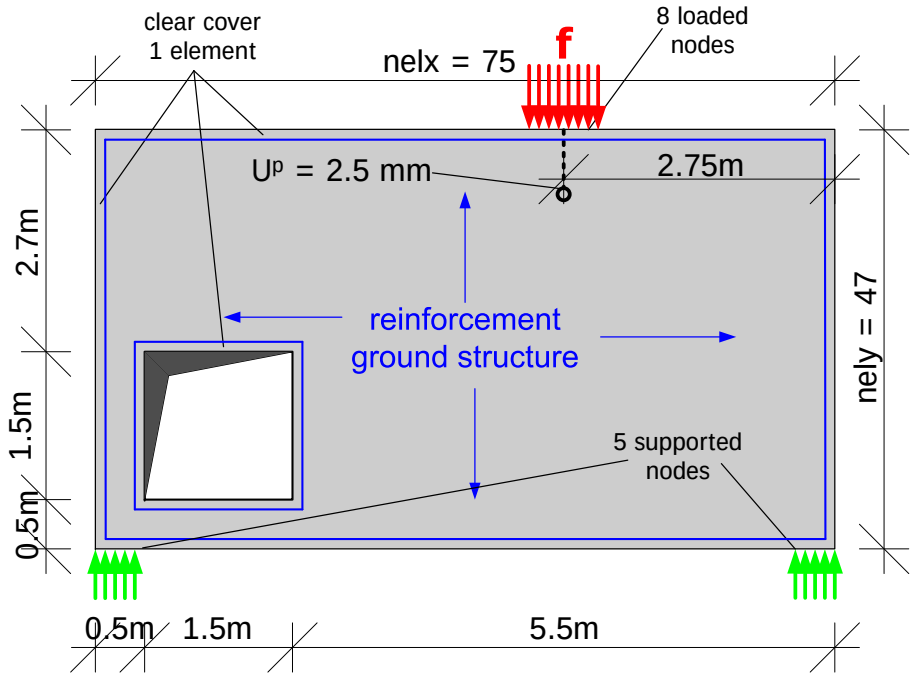

Figure 14: 2-D wall with opening: problem setting and computational model

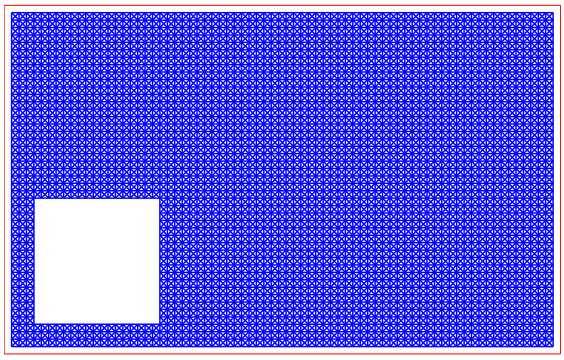

(a) Ground structure with uniform distribution of reinforcement, $\phi = -2.660 \times 10^{-3}$

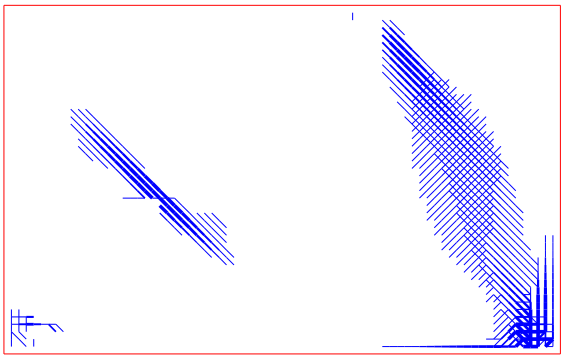

(b) Layout after 50 design cycles with $p_{bar} = 1.00$, $\phi = -3.489 \times 10^{-3}$

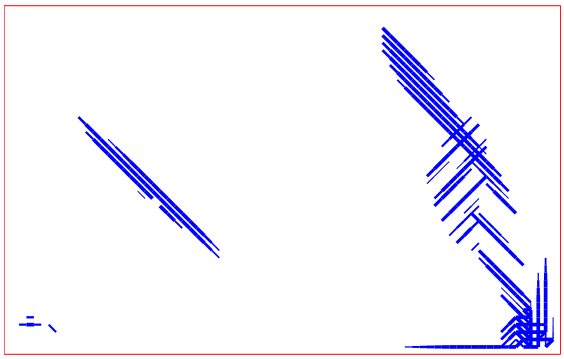

(c) Layout after 50 further design cycles with $p_{bar} = 1.25$, $\phi = -3.468 \times 10^{-3}$

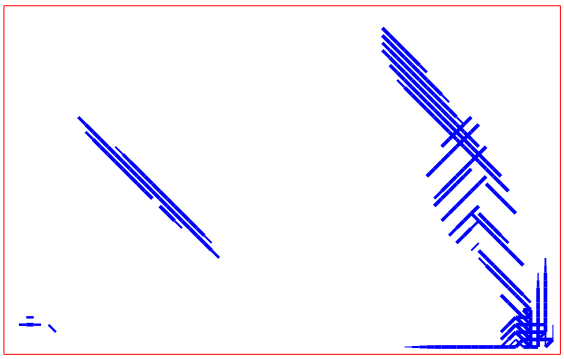

(d) Layout after 50 further design cycles with $p_{bar} = 1.50$, $\phi = -3.467 \times 10^{-3}$

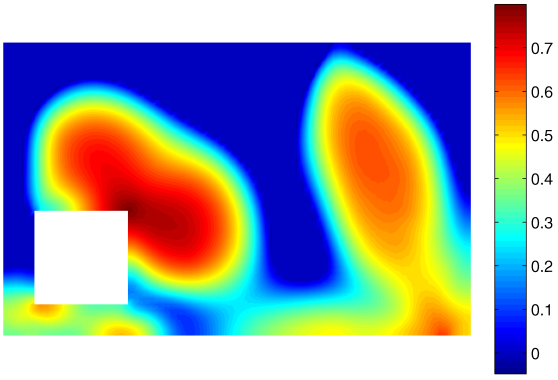

(e) Distribution of damage in the optimized design

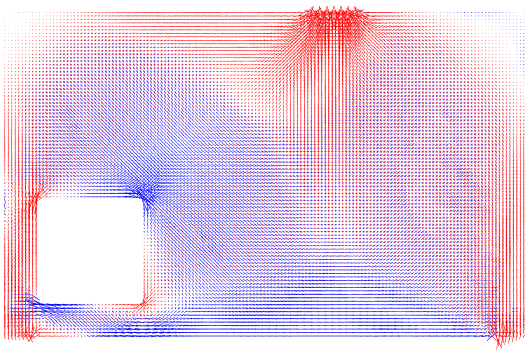

(f) Principal stress plot for the optimized design

Figure 15: Reinforcement layouts and response of the 2-D wall with opening, dense ground structure

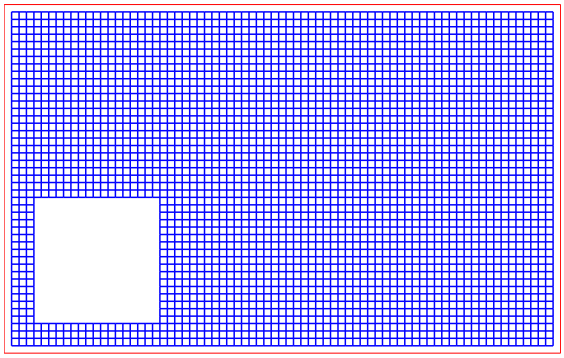

(a) Ground structure with uniform distribution of reinforcement, $\phi = -2.733 \times 10^{-3}$

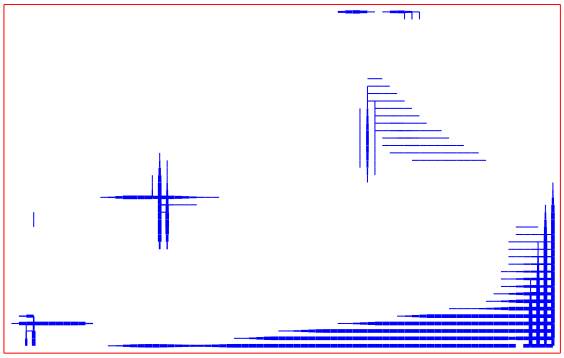

(b) Layout after 50 design cycles with $p_{bar} = 1.00$, $\phi = -3.156 \times 10^{-3}$

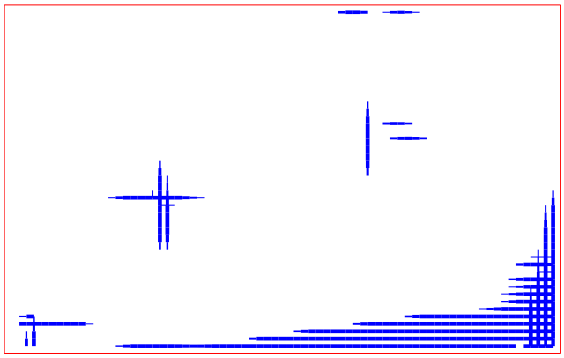

(c) Layout after 50 further design cycles with $p_{bar} = 1.25$, $\phi = -3.155 \times 10^{-3}$

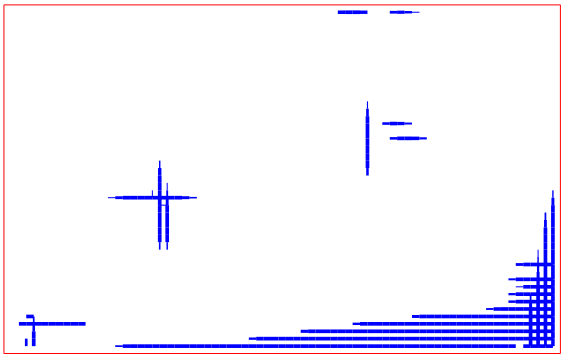

(d) Layout after 50 further design cycles with $p_{bar} = 1.50$, $\phi = -3.154 \times 10^{-3}$

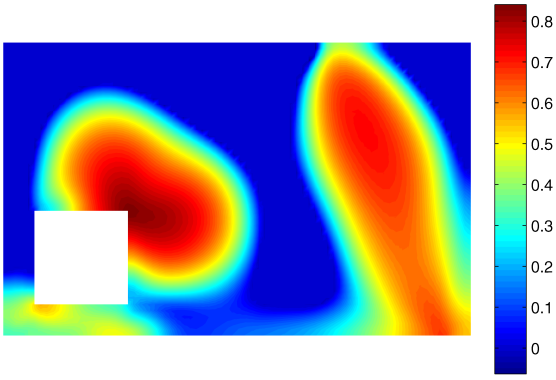

(e) Distribution of damage in the optimized design

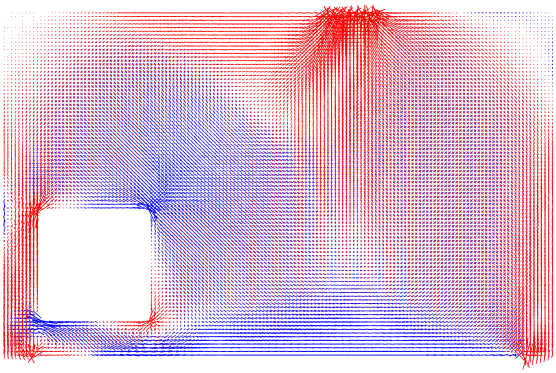

(f) Principal stress plot for the optimized design

Figure 16: Reinforcement layouts and response of the 2-D wall with opening, dense ground structure with rebars in Cartesian directions only

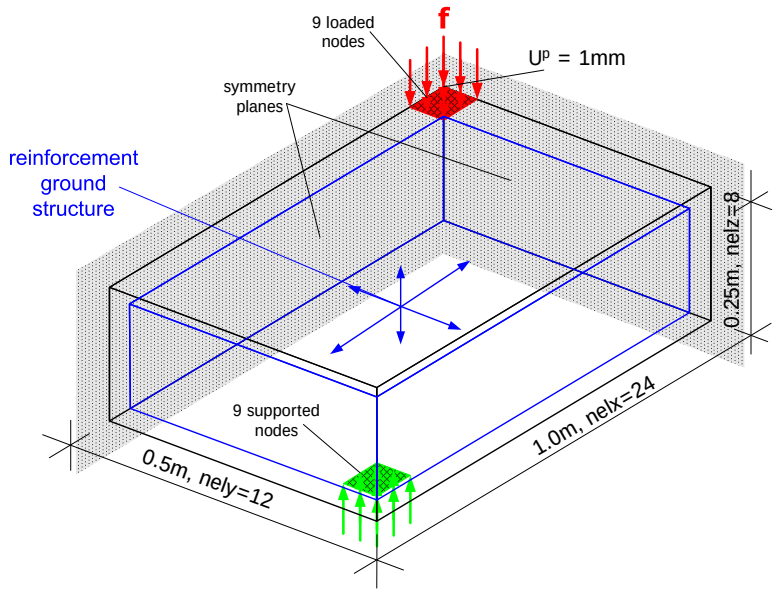

(a) Problem setting and computational model

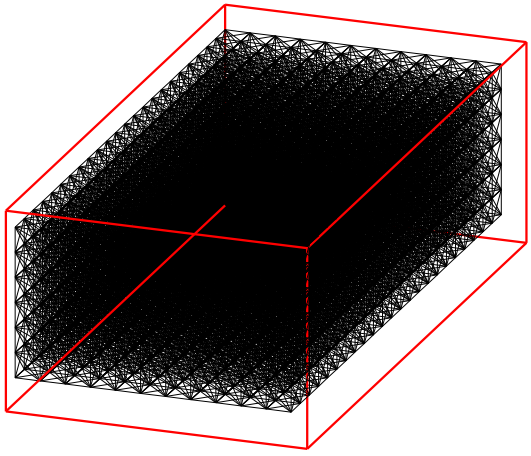

(b) Ground structure with uniform distribution of reinforcement, $\phi = -2.890 \times 10^{-6}$

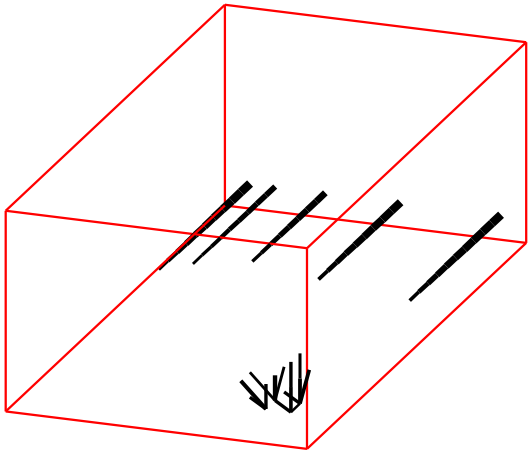

(c) Layout after 150 design cycles with gradual penalization, $\phi = -3.668 \times 10^{-6}$

Figure 17: 3-D pile cap example, double-symmetric quarter

are applied to the pile cap. Optimizing the distribution of rebars leads to a 27% improvement in load-bearing capacity compared to the initial design. Despite the relative simplicity of this test case, the prospects of utilizing this procedure as a digital design tool for complex 3-D structres are clearly demonstrated.

6 Discussion

A new approach for optimizing the distribution of reinforcement bars in structural concrete was presented. The main idea is to perform truss topology optimization where the ground structure consists of all acceptable positions of rebars. The ground structure is embedded into the continuum concrete domain where strain-softening response is considered by means of a nonlocal damage model. At the moment we focus on maximizing the load-bearing capacity at a given deformation level, i.e. maximizing the end-compliance for a certain prescribed displacement. Nevertheless, the procedure is general and other objectives, that are perhaps more suitable for reinforced concrete design, can be easily incorporated. The developed framework that combines nonlinear material modeling of concrete with an embedded truss ground structure as reinforcement provides the basis for optimizing the distribution of concrete and rebars simultaneously. This application is beyond the scope of the current study and will be addressed separately.

Observing the optimized layouts of reinforcement, it can be seen that rebars are positioned mainly in regions where concrete is severely damaged due to high tensile strains. Additionally, some reinforcement is used in compression in order to strengthen critical regions which are not necessarily highly damaged, for example in the vicinity of concentrated forces. This is of course related to the compliance objective and it is expected that for other goals, such as limiting cracking or reducing costs, somewhat different layouts may be generated.

At this point it is difficult to compare the optimized designs to the state of the art, namely strut-and-tie modeling. We apply only small deformations for initiating damage while strut-and-tie models assume a fully cracked concrete domain at the ultimate load state. Nevertheless, in the near future we intend to incorporate more advanced constitutive models for the concrete phase, which combine plasticity with either damage (e.g. Lubliner et al. [1989], Feenstra and de Borst [1996]) or fracture (e.g. Červenka and Papanikolaou [2008]). By considering a more realistic prediction of the concrete's response, we believe that this approach can be applied to both serviceability as well as ultimate limit states.

An attractive aspect of the suggested procedure is the fully digital work flow. Using CAD software, a detailed truss ground structure can be easily defined and exported to the finite element software. Automatic embedding of the truss elements is then performed, a rather straightforward operation if only structured grids are used. Once the optimized topology of rebars is found, it can be exported back to the CAD system and post-processed there for producing a final detailed drawing. Such a computational design tool can be very effective especially for designing complex 2-D and 3-D concrete structures.

7 Acknowledgements

The work of the first author was funded by the Danish Council for Independent Research | Technology and Production Sciences. The work of the second author was funded by Villum Fonden via the NextTop project. These supports are gratefully acknowledged. We wish to thank Claus B.W. Pedersen for several fruitful discussions and for his important comments. We also thank Krister Svanberg for the FORTRAN MMA code.

References

J.-L. Batoz and G. Dhatt. Incremental displacement algorithms for nonlinear problems. *International Journal for Numerical Methods in Engineering*, 14:1262–1267, 1979.

Z. P. Bažant, T. B. Belytschko, and T. Chang. Continuum theory for strain-softening. *ASCE Journal of Engineering Mechanics*, 110(12):1666–1692, 1984.

M. P. Bendsøe. Optimal shape design as a material distribution problem. *Structural Optimization*, 1:193–202, 1989.

M. P. Bendsøe and O. Sigmund. *Topology Optimization - Theory, Methods and Applications*. Springer, Berlin, 2003.

M. Bogomonly and O. Amir. Conceptual design of reinforced concrete structures using topology optimization with elasto-plastic material modeling. *International Journal for Numerical Methods in Engineering*, 2012. Accepted.

M. Bruggi. Generating strut-and-tie patterns for reinforced concrete structures using topology optimization. *Computers and Structures*, 87(23-24):1483–1495, 2009.

J. Červenka and V. K. Papanikolaou. Three dimensional combined fracture-plastic material model for concrete. *International Journal of Plasticity*, 24(12):2192 – 2220, 2008.

T. Chang, H. Taniguchi, and W. Chen. Nonlinear finite element analysis of reinforced concrete panels. *ASCE Journal of Structural Engineering*, 113:122–140, 1987.

P. Dombernowsky and A. Søndergaard. Three-dimensional topology optimisation in architectural and structural design of concrete structures. In *Proceedings of the International Association for Shell and Spatial Structures (IASS) Symposium*, Valencia, Spain, 2009.

D. C. Drucker and W. Prager. Soil mechanics and plastic analysis or limit design. *Quarterly of Applied Mathematics*, 10(2):157–165, 1952.

P. H. Feenstra and R. de Borst. A composite plasticity model for concrete. *International Journal of Solids and Structures*, 33:707–730, 1996.

fib Task Group 4.4. *Practitioners' guide to finite element modelling of reinforced concrete structures*. International Federation for Structural Concrete (*fib*), Lausanne, Switzerland, 2008.

J. Kato and E. Ramm. Optimization of fiber geometry for fiber reinforced composites considering damage. *Finite Elements in Analysis and Design*, 46(5):401–415, 2010.

J. Kato, A. Lipka, and E. Ramm. Multiphase material optimization for fiber reinforced composites with strain softening. *Structural and Multidisciplinary Optimization*, 39(1):63–81, 2009.

H.-G. Kwak and S.-H. Noh. Determination of strut-and-tie models using evolutionary structural optimization. *Engineering Structures*, 28(10):1440–1449, 2006.

J. Lemaître and R. Desmorat. *Engineering Damage Mechanics*. Springer, Berlin Heidelberg, 2005.

Q. Liang, Y. Xie, and G. Steven. Topology optimization of strut-and-tie models in reinforced concrete structures using an evolutionary procedure. *ACI Structural journal*, 97(2):322–330, 2000.

J. Lubliner, J. Oliver, S. Oller, and E. Oñate. A plastic-damage model for concrete. *International Journal of Solids and Structures*, 25:299–326, 1989.

P. Marti. Truss models in detailing. *Concrete International*, 7:66–73, 1985.

J. Mazars and G. Pijaudier-Cabot. Continuum damage theory - application to concrete. *ASCE Journal of Engineering Mechanics*, 115(2):345–365, 1989.

P. Michaleris, D. A. Tortorelli, and C. A. Vidal. Tangent operators and design sensitivity formulations for transient non-linear coupled problems with applications to elastoplasticity. *International Journal for Numerical Methods in Engineering*, 37:2471–2499, 1994.

C. D. Moen and J. K. Guest. Reinforced concrete analysis and design with truss topology optimization. In *Proceedings of the 3rd fib International Congress*, Washington D.C., USA, 2010.

R. H. J. Peerlings, R. de Borst, W. A. M. Brekelmans, and J. H. P. de Vree. Gradient enhanced damage for quasi-brittle materials. *International Journal for Numerical Methods in Engineering*, 39(19):3391–3403, 1996.

D. Phillips and O. Zienkiewicz. Finite element nonlinear analysis of concrete structures. *ICE proceedings*, 61(1):59–88, 1976.

J. Schlaich, K. Schafer, and M. Jennewein. Toward a consistent design of structural concrete. *PCI journal*, 32(3):74–150, 1987.

O. Sigmund and M. P. Bendsøe. Topology optimization: from airplanes to nano-optics. In K. Stubkjær and T. Kortenbach, editors, *Bridging from technology to society*. Technical University of Denmark, Lyngby, Denmark, 2004.

O. Sigmund and S. Torquato. Design of materials with extreme thermal expansion using a three-phase topology optimization method. *Journal of the Mechanics and Physics of Solids*, 45(6):1037–1067, 1997.

L. L. Stromberg, A. Beghini, W. F. Baker, and G. H. Paulino. Application of layout and topology optimization using pattern gradation for the conceptual design of buildings. *Structural and Multidisciplinary Optimization*, 43:165–180, 2011.

K. Svanberg. The method of moving asymptotes - a new method for structural optimization. *International Journal for Numerical Methods in Engineering*, 24:359–373, 1987.

M. Victoria, O. M. Querin, and P. Martí. Generation of strut-and-tie models by topology optimization using different material properties in tension and compression. *Structural and Multidisciplinary Optimization*, 44:247–258, 2011.